Development of electrically conductive concrete and mortars with hybrid conductive inclusions

Raphael Fulham-Lebrasseur, Luca Sorelli ⇑, David Conciatori

Department of Civil and Water Engineering, Université Laval, Canada

highlights

- 19 Mix designs of electrically concrete and mortars were tested.
- Best ECC mix design with graphene had an electrical resistivity under 200 Ω-cm.
- ECC mix design with reduced volume of graphite powder and steel fiber.
- Effect of water-to-cement ratio and drying curing was studied.

Keywords:
Electrically conductive concrete
Heated pavements
Concrete resistivity
Anti-icing
Compressive strength
Splitting tensile strength

abstract

Electrically Conductive Cementitious Composites (EC3) have been developed in the last decades to solve the drawbacks of conventional de-icing solutions, especially for urban regions with heavy snowfall where the cost of snow removal and accidents have been considerably increasing. This work aims at developing Electrically Conductive Concrete (ECC) and Mortars (ECM) at varying cement-to-water ratios (w/c) and curing conditions by combining electrically conductive inclusions, such as, carbon fibers, steel fibers, graphite powders, copper powder, and graphene. All samples were tested in terms of resistivity and mechanical strength. Moreover, the effect of thermal drying and long-term storage at 100% Relative Humidity (RH) on the electrical resistivity was studied. Among several mix designs with satisfactory electrical resistivity for de-icing applications, it was possible to develop an economically viable ECC mix design with a reduced volume of steel fibers and graphite powder with respect to that employed in previous works. Moreover, an ECC mix design with a quaternary mixture of conductive inclusions including a small amount of graphene exhibited a very low resistivity (177 Ω-cm) with a compressive strength of 24 MPa. For the ECC mix designs with low w/c ratio, the reduced capillary porosity seems to strongly affect the electrolytic ion conduction effect.

1. Introduction

In northern countries under severe climate conditions, snow and ice can strongly affect the urban transport with considerable delay, accidents and reparation costs. Moreover, the cost of snow removal has considerably increased in the last years due to the increase of precipitation worldwide and the cost of labor and materials [1,2]. As for examples, the snow removal budget at St. Paul Airport, Minnesota is about $4 million per year [3], while the snow clearing plan of Montreal is close to 160 M$/year [4]. The current method for roadways and sidewalks consists in the application of de-icing salts and clearing operations with mechanical plows, which has important drawbacks, such as: (i) corrosion of steel reinforcement of concrete structures [5], contamination of soils and groundwater [6]; and (iii) accidents and insurance costs [7]. Moreover, de-icing salts have a very low efficiency at very low temperature below −10 °C [7,8]. Nevertheless, an yearly amount between 10 and 20 million tons of salt has been used for snow removal in United States [6].

In the last decades, heating systems have been developed for snow removal, such as hydronic systems with a fluid (e.g. glycol) flowing into tubes embedded in concrete pavements [9]. However, hydronic systems have high cost of installation and pipe reparation, and their heating rate is relatively slow with considerable time to melt the snow [10]. The later can be solved by imposing a minimum temperature with a closed-loop control, but the operational costs increase significantly [9]. Electrical cables have been also widely used for heating concrete element. In spite of the low installation cost, this system has a strong energy consumption

⇑ Corresponding author.
E-mail address: Luca.sorelli@gci.ulaval.ca (L. Sorelli).

[11] and the temperature gradient around the cable can create thermal cracks in the concrete slab and reduces the snow melting efficiency [12].

As a recent solution, heating slab made of Electrically Conductive Concrete (ECC) have been developed by Joule effect [13–15].

In ECC conductive inclusions are added to concrete to create a continuous (percolated) path for electrical conduction [16]. The advantage of ECC heating system are the more uniform temperature distribution and low maintenance and reparation costs. The homogenized electrical resistivity of an ECC slab (ρ) can be calculated as follows $\rho = RA/L$, where A represents the cross-sectional area, L represents the distance between the two electrodes and R is the electrical resistance of the ECC material. The electrical conductivity σ is the inverse of the resistivity ρ. It is worth reminding that the electrical conduction is achieved by 2 phenomena in concrete: (i) the electron conduction through the percolated network of solid conductive phases (e.g., fibers, powders, aggregates, etc.); (ii) the electrolytic conduction through the motion of ions in the pore solution [17]. Based on previous works, the maximum resis- tivity of an ECC for an efficient deicing applications is about 1000 Ω-cm, which is two order magnitude less than that of normal concretes [5].

Table 1 summarizes the results of previous published results on ECC mix designs. Carbon Fiber (CF) have been successfully employed to develop ECC thanks to their high electrical conductivity [11,16,18]. Beaudoin et al. developed an ECC with a resistivity under 100 Ω-cm [19]. They also found it is possible reducing the CF volume content from approximately 5% to 3% by increasing the CF length from 1 mm to 3 mm. By optimizing the CF quality and its aspect ratio of CF, Abdualla and Sassani developed a ECC mix design with a very limited amount of CF (0.75%) with a resistivity of about 50 Ω-cm [11], which was applied for a pavement in Des Moines International Airport [7]. Notably, they found that the corrosion inhibitor admixture made of a calcium nitrite-based enhances the overall conductivity [16]. As drawbacks, CF are extre- mely expensive and with high-water absorption capacity, which reduces the workability of the fresh concrete and can compromise cast-in-place applications [16]. Banthia et al. investigated the use of hybrid fiber combining CF and Steel Fibers (SF) to reduce the minimum needed CF percolation volume [20]. Huo et al. also developed a ECC combining CF and SF with a satisfying resistivity, while also founding that larger aggregate size can reduce the elec- trical resistivity [21]. Yehia and Tuan developed a hybrid ECC with 15% Graphite Powder (GP) and 1.5 SF, which was employed for the the Roca bridge in Nebraska for a span of 146 m [22]. Wu et al. [23] investigated the combination of three conductive phases (i.e., steel fibers SF, CF and GP) obtaining a minimum resistivity of about 320 Ω-cm. They also verified the effect of dispersive agent, the size of the graphite particle and sand on electrical resistivity of concrete. Finally, intrinsic self-sensing concretes (ISSC) are a class of ECC in which the variation of the electrical resistance due to the damage is measured as a structural monitoring technique [24–26]. Previous works on ISSC showed that the water content has a remarkable nonlinear effect on the electrical conductivity [27–29] and thermal diffusivity [30].

In order to foster ECC technology, the objective of this work is threefold: (i) to develop mix designs of concrete ECC and mortars ECM with a hybrid combination of conducive inclusions, which includes small volume content of graphene; (ii) to verify the effect of curing conditions (e.g., temperature drying and high relative humidity storage); (iii) to develop a simplified model for predicting the resistivity.

Table 2
Information about raw materials used for ECC and ECM mix designs.

Material	Size/Type	Additional information
Coarse aggregates	2.5–10 mm	Crushed limestone
Fine aggregates	<2.5 mm	Natural sand
Silica 7030	30% retained by sieve mesh 70 (0.211 mm)	High purity industrial quartz sand
Silica 2075	75% retained by sieve mesh 20 (0.853 mm)	High purity industrial quartz sand
Silica fume	Densified micro silica	Eucon MSA
Cement	White Portland cement type GU	Federal white cement
Water	Demineralized water	–
Superplasticizer	Type A/F ASTM C494	Euclid Plastol 341
Methylcellulose	Viscosity at 2% 20 °C: 15 cPs	Used as a dispersive agent

2. Materials and methods

2.1. Raw and conductive materials

All mixes were made by using cement, water and superplasticizer (water reducer). For ECC, crushed stone and natural sand were used as aggregates, while quartz sand was used for ECM. Silica fume was also used in ECM mix to improve the bond with fibers and increase strength. Methylcellulose was used as a dispersive agent in mixes containing certain conductive materials. Specifications about raw materials are shown in Table 2. All conductive materials used in ECC and ECM mix are presented in Table 3. The Stainless Steel Fibers (SSF) used in this study has a maximum tensile strength of 344 MPa, while normal steel fibers (SF) has a maximum tensile strength of 450 MPa [33].

2.2. ECC mix-design, placing and curing

Table 4 reports the water-to-cement (w/c) ratio and the mass percentages (or volumetric fractions) of the raw materials for the 9 ECC mix designs. The mix designs were classified in 3 groups depending on their composition and measurements made, such as: Group G1 and group G2 differ by the choice of measurements done as explained in the following, while group G3 employs graphene and conductive aggregates with the same measurement made with group G2. Groups G1 and G2 were mixed with normal aggregates (crushed stone and sand), while Group G3 was mixed with conductive aggregates to replace normal aggregates. A small proportion of Graphene was added to mix ECC9 to see its influence on resistivity

Table 1 Comparison of the electrical resistivity (ϱ) for different volume content of conductive materials (V_f) from results in open literature and the ECC9 mix design of this work.

Reference	ρ (Ω-cm)	V_f (%)	Typical conductive filler [$\%_{vol}$]	w/c [–]	f_c [MPa]
[18,31]	100	n.a.	CF + carbonaceous particles	n.a.	n.a.
[11,16]	50	0.75	0.75%CF	0.56	40
[20]	820	1%	CF	0.3	n.a.
	359	3%	CF	0.3	n.a.
	78	5%	CF	0.3	n.a.
	187	3%	2%CF + 1%SF	0.3	n.a.
	512	3%	1%CF + 2%SF	0.3	n.a.
[21]	579	20.7%	0.7% CF + 20% SF	0.55–0.60	41
	38	20.7%	0.7% CF + 20% SF		40
[23]	322	5.40	1%SF + 0.4%CF + 4%GP	0.44	40
[32]	200	16.50	1.5% SF + 15%GP	n.a.	48

Table 3
Characteristics of conductive materials used in this work (n.a. = not available).

Material name	Size	Density (g/cm³)	Additional information	Electrical resistivity (Ω-m)	Reference
1. Conductive aggregates (CA)	d < 5 mm	2.04	FurseCEM™	n.a.	
2. Sieved Conductive aggregates (S CA)	d < 150 μm	2.04	FurseCEM™	n.a.	
3. Carbon fibers (CF)	L = 6 mm d = 7 μm	1.80	Grade 34–700	1.8×10^{-5}	[34]
4. Graphite powder (GP)	d < 20 μm	1.90	Synthetic	9.09×10^{-8}	[35]
5. Steel fibers (SF)	L = 13 mm d = 200 μm	7.86	Steel wire fibers	1.8×10^{-5}	[33]
6. Stainless steel fibers (SSF)	L = 19 mm d = 240 μm	7.95	Low carbon stainless steel	7.2×10^{-7}	[33]
7. Copper coated steel fibers (CuSF)	L = 13 mm d = 200 μm	7.86	Steel wire fibers	n.a.	
8. Copper powder (CuP1)	d < 425 μm	8.94	99.5% trace metals basis	1.67×10^{-8}	[36]
9. Copper powder (CuP2)	d < 75 μm	8.94	99% trace metals basis	1.67×10^{-8}	[36]
10. Graphene (Gn)	150 nm < d < 10 μm	2.20	Nanosheets	1×10^{-10}	[35]

Table 4
Mix designs in mass fraction (or volume fraction in parenthesis) for ECC groups: G1: ECC1R-ECC2; G2: ECC3-ECC6; and G3: ECC7-ECC9.

ID	w/c	Aggregates			CF (%)	GP (%)	SF (%)	SSF (%)	CuSF (%)	CuP1 (%)	Gn (%)
		Coarse (%)	CA (%)	Sand (%)							
ECC1R	0.50	34.2 (30)	–	34.4 (30)	–	–	–	–	–	–	–
ECC2	0.68	22.7 (18.0)	–	20.5 (16.3)	–	9.5 (10.6)	5.0 (1.35)	–	–	–	–
ECC3*	0.70	24.1 (18.4)	–	21.8 (16.5)	0.65 (0.73)	10.1 (10.9)	–	–	–	–	–
ECC4	0.68	24.1 (19.4)	–	21.8 (17.5)	–	10.1 (11.5)	–	–	5.3 (1.46)	–	–
ECC5	0.50	17.3 (18.7)	–	15.7 (16.8)	–	–	–	–	3.8 (1.40)	28.9 (9.3)	–
ECC6	0.68	23.3 (18.6)	–	21.1 (16.8)	–	9.8 (11.0)	–	5.1 (1.38)	–	–	–
ECC7	0.60	11.6 (9.1)	8.81 (9.1)	21.0 (16.4)	–	9.7 (10.8)	5.1 (1.36)	–	–	–	–
ECC8	0.60	–	18.1 (18.2)	21.6 (16.4)	–	10.0 (10.8)	5.2 (1.36)	–	–	–	–
ECC9**	0.60	–	18.1 (18.2)	21.5 (16.3)	–	10.0 (10.8)	5.2(1.36)	–	–	–	0.1 (0.1)

* Methyl cellulose was added to mix ECC3 to disperse CF.
**Methyl cellulose and isopropyl alcohol 70%USP were added to the graphene powder before incorporation into the mix-design to disperse it in mix ECC9.

and mechanical strength. In most of the mix design the volume ratio of cement: sand:aggregate is close to 1:1:1 which was found to be a good proportion [21]. The GP content was kept 30% less than the one developed by [13] in order to minimize

The surface texture of ECC mix designs was clearly different. For sake of completeness, Annex A shows the photos of the different surface texture of the mix designs ECC and ECM studied in this work. All the samples containing GP have a black color matrix. In general, the limestone aggregate seems homogenously dis- tributed in the ECC matrix. In particular, the mix designs ECC8 and ECC9 the car- bonaceous conductive aggregates are uniformly distributed in the black matrix embedding the few remaining sand inclusions. The fibers CuSF and SF can be clearly observed in mix designs ECC2 to ECC9, with exception of ECC3 that has CF which are very small and have the same color of the matrix. The pink color of the ECC5 is due to the CuP matrix inclusions.

2.2.1. Placing

All mix designs were mixed with a ½ HP Hobart mixer model A-200 at an agitator speed of 107 RPM with a bowl of 20 qts (18.9 l). Every mix design was casted in two cylindrical molds of 200 mm of height and 100 mm of diameter. All mix designs were made following the same mixing sequence. The dry ingredients (aggregates, cement and different powders) were mixed together for 5 min. Water and superplasticizer were then added in about 1 min 30 s. Once the fresh concrete or mortar was rather fluid, the different fibers were added (with exception of the reference mix ECC1R). Fibers were mixed for 3 min before casting. Each cylindrical mould was filled in 3 shots, each one compacted 25 times with a steel rod. For the mix designs with GP, which were characterized by high rigidity, 25 additional hits of rubber hammer were necessary to vibrate and fill the cylindrical moulds.

2.2.2. Curing

All cylinders were protected with a wet blanket in ambient air for 24 h. After demolding, they were placed for 6 days in a 100% Relative Humidity (RH) with a temperature of about 23 °C. A temperate thermal treatment (TT) was then applied, which consists of a storage in water at about 70 °C for 3 days. The TT curing provides better early age compressive and tensile resistance [37], as well as reduced shrinkage and creep [38]. The accelerated hydration is also beneficial to guarantee earlier stable electrical resistivity.

2.2.3. Absorption tests for conductive powders

The mix designs require a larger amount of water as part of it is absorbed by powders. A test procedure was set-up to estimate the water absorption of powders. First, a funnel was placed over a vacuum pump with a high retention filter in it. The filter was wetted with demineralized water. Powder was then added in the filter and wetted with a large amount of water. The pump was turn on to extract all free water from the mix-design. Then, the wet powder was extracted from the funnel and separated in 3 aluminum weighing dishes. Their weight with wet powders was also measured. The 3 samples were stored in a stove at 110 °C and were weighed every 24 h until there was no weight changes. The absorptions tests were conducted on GP, CA, SCA and CuP2 to make mix design for ECM.

2.3. ECM mix designs, placing and curing

2.3.1. Mix table

Table 5 below shows the 10 ECM mix designs in mass percentage (or volumetric fractions in parenthesis). ECM mix designs were separated in two groups, depending on the size of the cylinders they were casted: G1: ECMR-ECM3 with diameter 50 mm and height 100 mm and G2: ECM4-ECM9 with diameter 100 mm and height 200 mm. In mixes ECM2 and ECM3, CA were sieved to increase the specific area. The powder used was the one passing through ASTM 100 sieve (0.15 mm). CuP2 was used in ECM9 mix design instead of CuP1 to have a larger specific area.

As for the ECC mix designs, the surface texture of ECM looks rather heterogeneous (see photos in Annex A). Qualitatively speaking, group G2 are darker than group G1 because of the high carbon content, with exception of ECM9, which has CuP instead of GP. SF are clearly visible and are homogeneously distributed in the matrix. CF contained in mix ECM1 to ECM 5 are not visible at naked eye.

2.3.2. Casting and placing

Group G1 mix designs were made in a 1/2HP Hobart mixer model A-200, at an agitator speed of 107 RPM with a bowl of 20 qts (18.9 l). Group G2 mix designs were made in a 1/6HP Hobart mixer model N50, at an agitator speed of 136 RPM with a bowl of 5 qts (4.7 l). Group G1 samples were casted in two cylindrical molds of 200 mm of height and 100 mm of diameter while group G2 were casted in two cylindrical molds of 100 mm of height and 50 mm of diameter.

All mixes were carefully prepared following the same mixing sequence. All the dry ingredients (silica sand, silica fume, cement and different powders) were mixed together for 5 min. Water and superplasticizer were then added in 1 min 30 s. Once

Table 5
Mix designs in mass volume percentage (or volume fraction in parenthesis) for ECM groups, such as, G1: ECMR-ECM3; Group G2: ECM4-ECM9.

ID	w/c	Aggregates			SCA	CA	GP	CuP2	CF	SF	Gn
		Sand No.7030 (%)	Sand No.2075 (%)	Silica Fume (%)	(%)	(%)	(%)	(%)	(%)	(%)	(%)
ECMR	0.22	38.8 (27.8)	9.6 (6.9)	7.7 (30.4)	–	–	–	–	–	5.0 (1.20)	–
ECM1	0.42	34.6 (23.7)	8.5 (5.8)	6.9 (25.9)	–	–	4.2 (4.0)	–	0.4 (0.4)	5.2 (1.2)	–
ECM2	0.24	36.7 (26.3)	9.0 (6.5)	7.3 (28.7)	4.3 (4.0)	–	–	–	0.4 (0.4)	5.0 (1.2)	–
ECM3	0.32	35.6 (25.0)	8.8 (6.2)	7.1 (27.3)	2.2 (2.0)	–	2.0 (2.0)	–	0.4 (0.4)	5.1 (1.2)	–
ECM4	0.54	32.3 (21.7)	7.9 (5.3)	6.4 (23.7)	–	–	6.4 (6.0)	–	0.4 (0.4)	5.3 (1.2)	0.31 (0.25)
ECM5	0.88	27.8 (17.8)	6.8 (4.4)	5.5 (19.5)	–	–	11.2 (10.0)	–	0.4 (0.4)	5.6 (1.2)	–
ECM6	0.59	28.1 (19.3)	6.9 (4.7)	5.6 (21.1)	–	11.2 (10.0)	5.2 (5.0)	–	–	6.5 (1.5)	–
ECM7	0.42	29.7 (21.0)	7.3 (5.2)	5.9 (22.9)	–	10.9 (10.0)	5.1 (5.0)	–	–	6.3 (1.5)	–
ECM8	0.57	23.9 (16.7)	5.9 (4.1)	4.8 (18.2)	–	22.1 (20.0)	5.1 (5.0)	–	–	6.4 (1.5)	–
ECM9	0.83	25.1 (24.9)	6.2 (6.1)	5.0 (27.2)	–	–	–	34.0 (10.0)	–	4.5 (1.5)	–

Table 6
Maximum and minimum w/c ratios by weight by considering the powder absorption capacity.

ECC				ECM			
ID	w/c	$(w/c)_{min}$	ρ_{TT} (Ω cm)	ID	w/c	$(w/c)_{min}$	ρ_{TT} (Ω cm)
ECC1R	0.50	0.50	5257	ECMR	0.22	0.22	38,319
ECC2	0.68	0.23	286	ECM1	0.42	0.22	4408
ECC3	0.70	0.22	163	ECM2	0.24	0.22	30,539
ECC4	0.68	0.15	288	ECM3	0.32	0.22	10,126
ECC5	0.50	n.a.	304	ECM4	0.54	0.22	890
ECC6	0.68	0.19	402	ECM5	0.88	0.22	515
ECC7	0.60	0.10	242	ECM6	0.59	0.22	547
ECC8	0.60	0.04	215	ECM7	0.42	0.22	2352
ECC9	0.60	0.04	177	ECM8	0.57	0.22	957

the mix was fluid enough, fibers were added. Fibers were mixed for 3 min, and the mix was casted. Each cylinder was filled in three shots of about a third of the cylinder volume and compacted 25 times with a steel rod. For the mix using GP, 25 hits of rubber hammer were necessary to vibrate the cylinders to fill them correctly. For mix ECM9, extra water was necessary because the mix was still too dry, even if absorption tests to know the total needed amount of water were conducted on CuP2.

2.3.3. Curing

All cylinders were covered with a wet blanket in ambient air for 48 h due to high dosage of superplasticizer. After demolding, they were placed 5 days in a100% RH and a temperature of about 23 °C to avoid risk of early age cracking. The sample were then cured with a temperate thermal treatment (TT), which consists of an immersion under water for 3 days at temperature controlled of 70 °C (see part 2.2.3).

2.4. Methods

2.4.1. Electrical resistivity measurements

All the electrical resistivity measurements were made using a concrete bulk electrical resistivity testing device, which is commercially available under the name Giatec RCON2™. The concrete (or mortar) cylinder is placed between two parallel electrodes. A wet sponge and conductive gel were applied at each end of the cylinders to insure a good contact with electrodes. An alternative current (I) source aliments the electrodes at different frequencies. The potential drop (ΔV) is measured, and the resistance (R) is calculated with the Ohm's law:

$$\Delta V = RI \quad (2)$$

The electrical resistivity is then calculated with Eq. (1). The machine gives the value of electrical resistivity, in Ω-m, for a cylindrical sample measuring 4'' × 8'' (203.2 mm of height and 101.6 mm of diameter). Each specimen was measured 10 times (5 times diameter and 5 times height). A correction factor was applied to consider the effective diameter and height of the G2: ECM4-ECM9 sample.

2.4.2. Electrical resistivity measurements for ECC

For ECC group G1, electrical resistivity was measured at 4 different consecutive conditions, such as: (i) ''WET70'' just after the TT treatment (which was at 70 °C for 3 days in water as aforementioned); (ii) ''DRY70'' after drying in air at 70 °C for 24 h as done by previous researchers [17]; (iii) ''DRY20'' after that the specimens were cooled down at 20 °C for 24 h; (iv) ''Long-term at 100% RH'' after a long period (56 days) of storage at 100% RH and room temperature (20 °C).

For the ECC group G2 and G3, electrical resistivity was measured at 5 different consecutive conditions, such as: (i) ''WET70'' right after the TT; (ii) ''WET20'' after 24 h of immersion in water at 20 °C; (iii) ''DRY70'' after drying in air at 70 °C for 24 h as done by previous researchers [17]; (iv) ''DRY20'' after that the specimens were cooled down at 20 °C for 24 h; (v) ''Long-term at 100% RH'' after a long period (56 days) of storage at 100% RH and room temperature (20 °C).

2.4.3. Electrical resistivity measurements for ECM

For both groups G1 and G2 of ECM, samples were not dried because the available water was minimal to hydrate the amount of cement, i.e., no free water is assumed. Thus, electrical resistivity was measured at 4 different consecutive conditions: (i) ''WET70'' after the thermal treatment at 70 °C; (ii) ''After 24 h at 20 °C'' after samples were stored for 24 h in a room at ambient humidity and temperature at 20 °C; (iii) ''After 48 h at 20 °C'' was measured 24 h later than previous measurements at same conditions; (iv) ''Long-term at 100% RH'' after 28 days of storage at 100% RH and room temperature (20 °C).

2.4.4. Splitting tensile and compressive strength for ECC and ECM

Due to the large number of samples tested and the cost of raw materials, each test was conducted only on a limited number of samples. However, the test repeatability was rather satisfactory thanks to the careful control of the fabrication procedure reduce, e.g., the difference between the mean resistivity of 2 samples and the single measurements was less than 5% for all samples.

Both tests were carried out by a 5000 kN hydraulic press. Due to the high cost of raw materials only one and two cylinders were used for compressive strength for ECC and ECM, respectively. Cylinders were first cut using a concrete saw and then grinded on both sides. The compressive strength tests for ECC were made in accordance with ASTM Standard C39 [39] at a loading rate of 2000 N/s which corresponds to 0.25 MPa/s. However, the loading rate was 8000 N/s (1 MPa/s) and 2000 N/s (1 MPa/s) for ECM group G1 and G2, respectively. The splitting tensile strength tests were conducted on 1 sample of each mix of ECC in accordance with ASTM Standard C496 [40].

2.4.5. Simplified prediction of ECC resistivity

Several works have been attempted to develop rather complex homogenization model to predict the electrical conductivity or resistivity of a composite cementitious material with conductive inclusions, such as CF or SF [17,41,42]. Such models are difficultly suitable for composite with multiple inclusions as they do not well consider inclusions interaction and their shape effect. It is expected that such simplified model applies for a small volume content of conductive materials of few percentages. In this preliminary work, a simplified method is proposed by a simplified average operation with back analysis of the resistivity of the raw materials from Eq. (3) and Eq.(4). The resistivity of the employed conductive inclusions was taken from

the values reported in Table 3 and were estimated for those not available. In the lack of availability of their experimental value, the resistivity values for natural sand and crushed limestone were adjusted to arrive to realistic orders of magnitude. Values used for cement paste were typical values. The porosity in Eq. (3) was calculated by classical Power's volumetric model for cement paste [43]. The values of solution's resistivity (0.35 Ω-m) were taken as measured values of a previous work with similar concretes [44]. Specimens were considered at a saturation of 100%.

$$\rho_s = \rho_{cp} \times \left(1 - \sum V_i\right) + \sum \rho_i \times V_i \quad (3)$$

$$\rho_{tot} = \rho_{sol} \times V_p + \rho_s \times (1 - V_p) \quad (4)$$

where ρ_s is the solid resistivity, ρ_{cp} is the resistivity of cement paste, ρ_i is the resistivity of inclusions, V_i is the volumetric fraction of the inclusions, ρ_{sol} is the resistivity of the interstitial solution, V_p is the volumetric fraction of the pores calculated with Power's model and ρ_{tot} is the total resistivity.

3. Results and discussion

3.1. ECC results and discussion

3.1.1. Resistivity tests

Each test was conducted on two samples. The repeatability was satisfactory as the difference between the mean values and the measurements was less than 10%. The de-icing application threshold has been traced in red on each ECC resistivity figure. Presented results are the average of the two samples.

Resistivity measurements made on ECC group G1 are shown in Fig. 1. The ECC samples are more electrically conductive (lower electrical resistivity) when they are wet and when they are at ahigher temperature. As found in previous works [20,24,27], when the sample is wet, electronic and electrolytic conduction are combined, and the concrete is more conductive. On the other hand, when the sample is dried, only electronic conduction is possible, which explains that the resistivity is higher. Interestingly, ECC samples seem to recover their electrical conductivity after the storage at a moisture of 100% RH. The reference mix ECC1R has no conductive material, which explains its very high electrical resistivity. ECC2 provides a suitable resistivity as it meets the usual values that are required for de-icing applications, which is being under 1000 Ω-cm.

Fig. 2 shows the resistivity measurements made on ECC group G2. Again, under high temperature and wet condition, the electrical resistivity of all mix designs decreases. The only exception was mix ECC3, which is more conductive at measurement WET20 than at WET70. The lowest resistivity of ECC3 confirmed the high efficiency of carbon fibers in providing electrical conductivity. Interestingly, ECC4 exhibited the greatest recovery of electrical

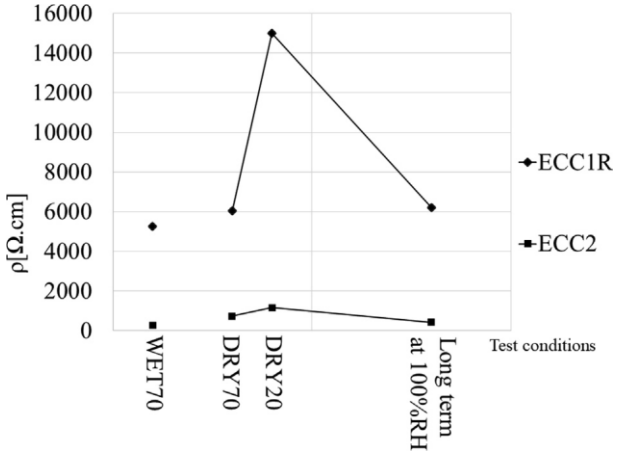

Fig. 1. Electrical resistivity measurements for ECC group G1.

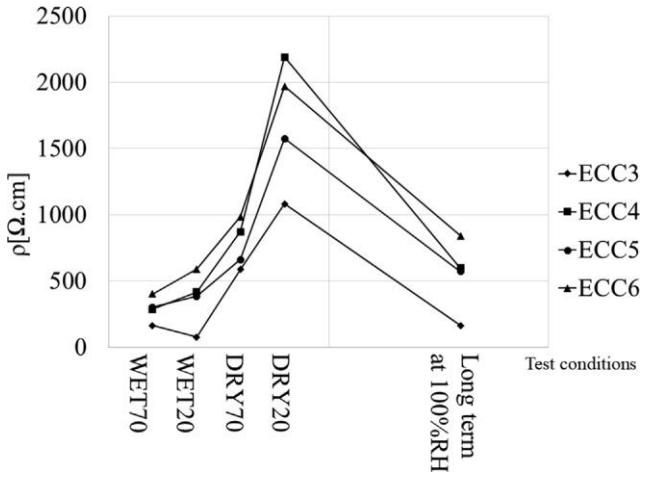

Fig. 2. Electrical resistivity measurements for ECC group G2.

resistivity after long term 100% RH curing. The higher graphite content may have involved a greater amount of available water and, in turn, increased the porosity. Thus, in the water recovery cycle, water can fill back the pores, which contributes to the observed recovery of the electrolytic conduction.

Fig. 3 shows the resistivity measurements made on ECC group G3. All the curves showed a similar behavior and low resistivity. Yet, wet conditions and high temperature decreased the electrical resistivity. The electrical conductivity was recovered at long term after 100% RH curing for all mix designs.

Compared to ECC8, the contribution of the relatively small amount of graphene (Gn) in mix ECC9 reduces the electrical resistivity of 19% and 58% for WET70 and DRY20 conditions, respectively. In spite of the small volume addition of graphene, the effect on the resistivity is noteworthy, especially for dry condition. It is worth mentioning that graphene (which is fundamentally a single layer of graphite) is characterized by a extremely high con- ductivity, which is 2 order of magnitude greater of that of graphite. Interestingly, other works have found a similar effect of graphene on the thermal conductivity of cement-based materials [45] and on their piezoelectric effect [46], which are perhaps due to synergistic effect with the other conductive inclusions.

The replacement of the half of coarse aggregates by CA in mix design ECC7 in comparison with ECC2 (same ingredients but without CA) had a small influence on short-term resistivity conditions

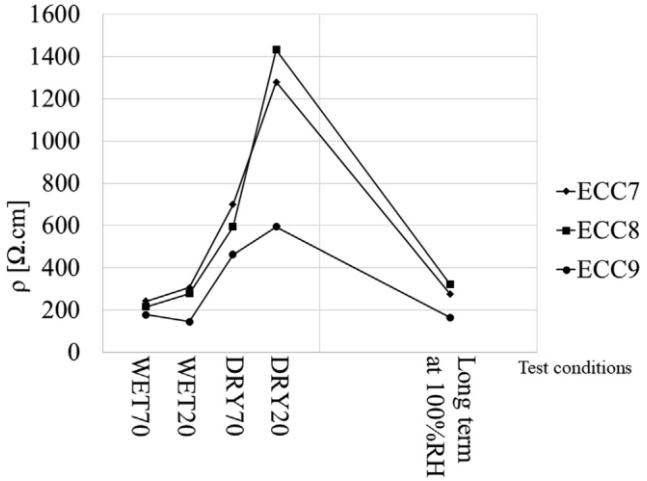

Fig. 3. Electrical resistivity measurements for ECC group G3.

(<16% of reduction), but a significant effect at long term (>35% of reduction). The replacement of all the coarse aggregates by CA in mix design ECC8 in comparison with ECC2 had a significant influence on resistivity (about 25% of reduction), except for DRY20 condition.

The effect of curing on the electrical resistivity is mainly due to the effect of the reduction of capillary water which is needed for the electrolytic ion conduction within the conductive porous medium. The long-term curing at 100%RH is able to refill the capillary porosity and rescue the electrical conductivity.

3.1.2. Splitting tensile and compressive strength

Fig. 4a shows the splitting tensile strength (f_{sp}) and compressive strength (f'_c) of ECC mix designs. In general, the GP addition reduces the compressive (f'_c) and splitting tensile strength (f_{sp}), while the presence of steel fibers (SF) seems to compensate such reduction. Notably, Mix ECC5 has the highest compressive and splitting tensile strength due to the lower w/c ratio. Mix ECC6 with stainless steel fibers has a lower splitting tensile strength than other mix designs containing fibers and GP, which is perhaps due to the lower tensile strength of the SSF with respect to SF. Also, the longer length of SSF made difficult to disperse homogeneously [7]. It can be observed that CF contained in mix ECC3 helps for tensile strength, but not for compressive strength, as observed by other researchers [47]. The use of alcohol and methylcellulose used in mix ECC9 might have reduced f'_c and f_{sp} in comparison with ECC8, which has the same composition, but without 0.1% of graphene.

Fig. 4b compares the resistivity after thermal treatment ρ_{TT} with the compressive strength f'_c for all ECC mix designs. The mix design ECC5 with copper powder showed the highest com- pressive strength (44.9 MPa) and acceptable resistivity (about 304 Ω-cm). Instead, ECC9 which combines GP, SF and Gn had a slightly greater resistivity of the ECC3 with 0.65% of CF (163 Ω cm vs. 177 Ω cm) and slightly higher compressive strength (24 MPa vs. 17.8 MPa).

3.2. ECM results and discussion

3.2.1. Resistivity tests

Due to the wide research campaign, the test repetition was limited to two samples. However, the measurement repeatability was rather satisfactory thanks to a careful control of the fabrication procedure. For instance, the difference between the mean resistivity of 2 samples and the single measurements was less than 5%. The mean resistivity measurements made on ECM groups 1 and 2 are shown on Fig. 5. The de-icing application threshold has been traced in red on Fig. 5(b), but not on Fig. 5(a) because of the order of magnitude of results. All the curves follow the same behavior, they are more conductive at the end of the TT because of the high temperature, and they stabilize when they cool down. Once they regain a certain amount of water at long-term their resistivity reduces, but not as much as the ECC ones. Absorption experimentations led to a reduced water amount, which resulted in a reduced porosity. ECM are less conductive than ECC because of this reduced porosity, which allows less electrolytic conduction. Mix ECM4 and ECM5 are below the 1000 Ω-cm limit for the de-icing application, while ECM6 and ECM8 are barely over the limit when they are cooled and dry. Other mix designs did not achieve a electrical resistivity lower than 1000 Ω cm. ECM5 is characterized by the lowest resistivity, but also the lower compressive strength (see part 3.2.2) due to the high water-cement ratio. This mix required more water and superplasticizer because of the graphite content even if calculations were made with absorption results. Notably, mix ECM4 with small amount of graphene has a relatively high compressive strength and a significantly low resistivity. As found in previous studies [7], ECM showed higher electrical resistivity than ECC presented in previous section. In particular, Hou et al. found that replacing coarse aggregate with finer sand at the same total amount of total aggregate increases the electrical conductivity of an order of magnitude [21]. Thus, the finer sand employed in ECM mix designs contributed to a denser matrix (i.e., with less porosity at the micrometer scale) which may have limited the electrolytic conduction.

3.2.2. Compressive strength

Fig. 6a shows the compressive strength of the ECM mix designs. As general trend, when the powder content is higher, the resistivity is lower, but the compressive strength is lower. The mix design ECMR can be classified as a Ultra High Performance Fiber Reinforced Concrete (UHPFRC) [48] as the mean compressive strength is greater than 120 MPa. Mix designs ECM5 and ECM9 required more water than other mix designs (w/c of 0.88 and 0.83 respectively), which explain their relatively lower mechanical strength.

Fig. 6b compares the resistivity after TT ρ_{TT} with the compressive strength f'_c for the ECM mix designs showing that several 5 on 9 of them are not suitable for deicing applications as ρ is too high. On the other hand, Fig. 7c shows the ECM mix designs which are suitable for deicing applications (e.g., ρ < 1000 Ω cm). It is noted that the mix design ECM6 with CA, GP and SF has relatively high comprēssive strength (50.8 MPa) and low resistivity (547 Ω cm). The mix design ECM5 with SF, CP and SF has similar resistivity (515), but lower compressive strength (24.5 MPa).

3.3. Absorption tests with powders

In general, small particles with higher specific surface area absorb more water. In particular, the smallest particles GP absorb the greater amount of water, followed by CuP2 and finally the SCA. CA conductive aggregates absorb a little more water than

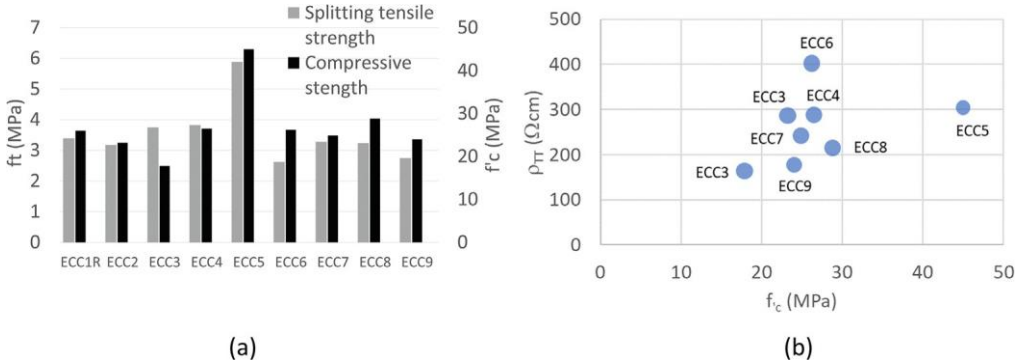

Fig. 4. (a) Splitting tensile (f_t) and compressive strength (f'_c) of ECC mix designs; (b) Resistivity after TT ρ_{TT} vs. f'_c for ECC mix designs.

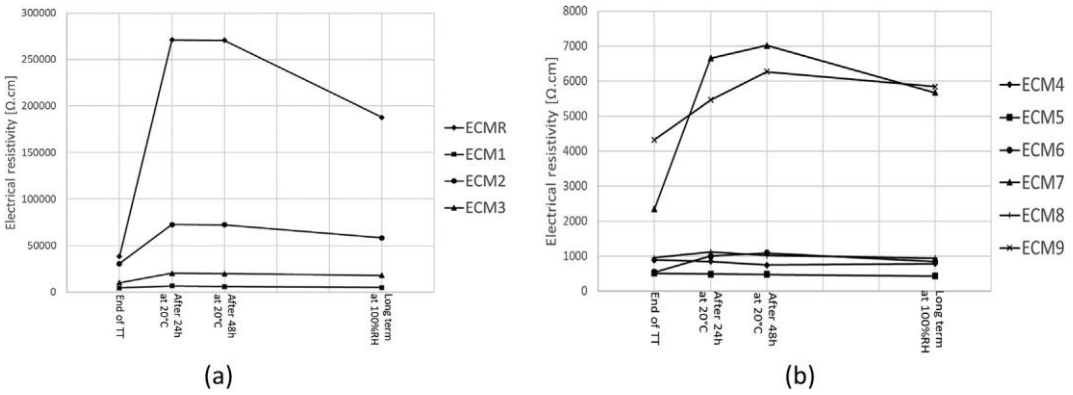

Fig. 5. Electrical resistivity measurements of ECM: (a) group G1; (b) and group G2.

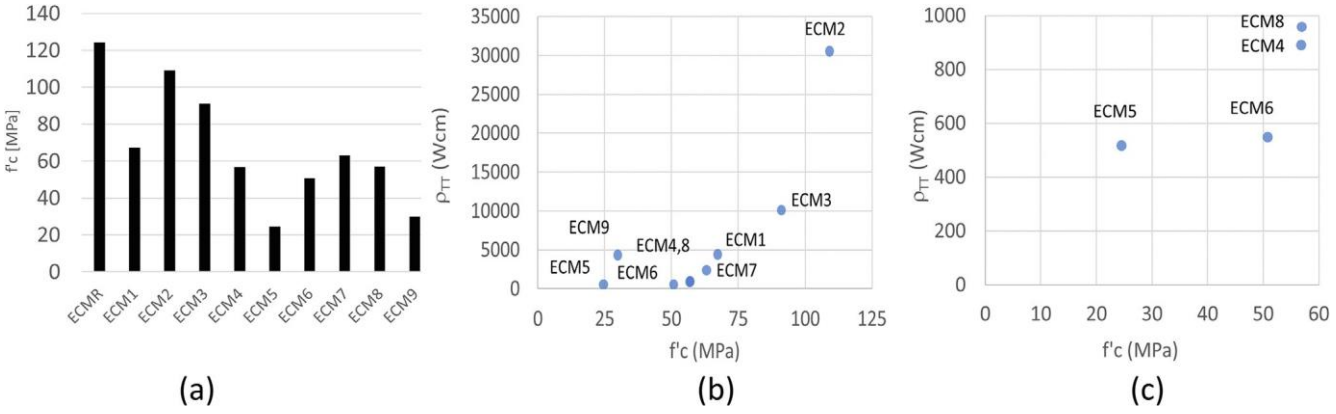

Fig. 6. (a) Compressive strength f'_c of ECM mix designs; (b) resistivity (ρ_{TT}) vs. compressive strength (f'_c) of the ECM mix design (c) zoom on ECM mix designs with resistivity (ρ_{TT}) lower than 1000 X-cm.

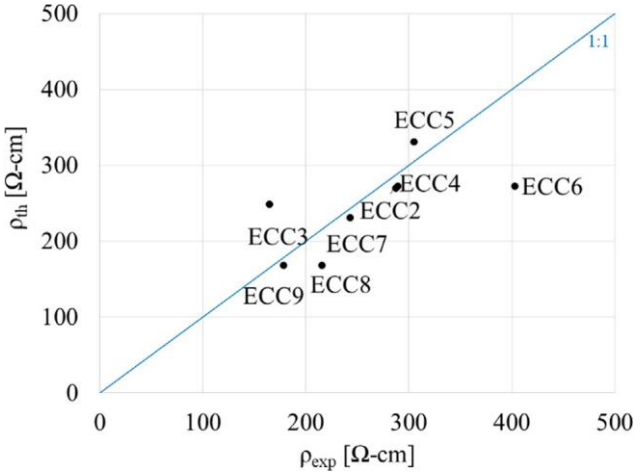

Fig. 7. Comparison of the theoretical and measured resistivity for ECC at WET70 condition.

SCA, which is probably due to the intrinsic porosity of the material. Based on the absorption test result, we estimated: 1.20 g/g for GP, 0.19 g/g for CA, 0.12 g/g for SCA and 0.21 g/g for CuP2. Table 6 summarizes the maximum w/c ratio (by weight) as provided and the minimum $(w/c)_{min}$ as calculated by assuming that all the water absorbed by the conductive materials is retained during the entire hydration, which can be considered as an upper bound case. In addition, for sake of completeness, the resistivity after the TT ρ_{TT} have been reported in the same table. The real w/c ratio is between those 2 values depending on the stability of the water absorbed layer during the hydration process. As for ECM, the $(w/c)_{min}$ = 0.22 was the same for all mix design as a fixed parameter for this study.

3.4. Simplified prediction of ECC resistivity

As for the simplified modeling, Fig. 7 compares the predicted and measured resistivity of ECC mix designs containing conductive materials for WET70 condition. The predicted values were obtained by best-fitting the resistivity of raw materials (sandstone and crushed limestone) and the resistivity of cement paste, ρ_{cp}, in Eqs. 3 and 4 for WET70 condition. The electrical resistivity values of conductive materials were taken from literature, which were reported in Table 3. The best-fitting ρ_{CP} value is 600 Ω-cm, while the best-fitting values for sandstone and crushed limestone are 50 Ω cm and 1500 Ω-cm, respectively. Those values are in good agreement with other researchers [19]. In spite of the simplicity of the model, the comparison between the predicted and measured points are satisfactorily close to the equality line (1:1) with a mean error on the predicated resistivity of about 17%. It is worth noticing that the values ECC3 and ECC6 are less satisfactory (errors of 65% and 35% respectively). Note that ECC3 mix design showed a very low resistivity due to the high electrical conductivity of carbon fibers.

3.5. Correlation analysis

Fig. 8a presents the compressive strength in function of w/c for ECC and ECM. As found in previous researches for high

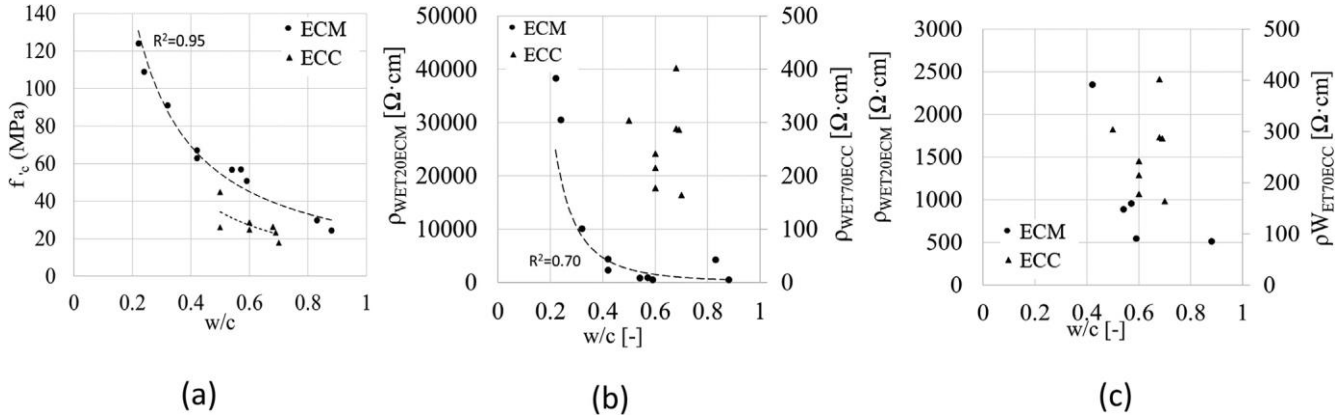

Fig. 8. (a) Compressive strength in function of w/c for ECC and ECM (b) Resistivity in function of w/c for ECC and ECM; (c) zoom of the previous figure.

performance concrete [49], the compressive strength of both ECC and ECM decreases when the w/c ratio increases. A power function showed a good determination coefficient (R^2 = 0.95) with the experimental results ρ vs. f'_c for the ECM mix designs. On the other hand, the ECC systems did not show a good correlation R^2 = 0.49 over a lower range of w/c ratio. Perhaps, the interaction transition zone (ITZ) around the aggregate may have reduced the overall strength and the correlation between ρ vs. f'_c as found in previous works [50,51].

Fig. 8b presents ρ vs. w/c for ECC and ECM systems at condition WET70. An acceptable correlation with a power function is visible for ECM (R^2 = 0.70), while no correlation is found for ECC. As for ECM, a significant increase of the resistivity is visible when the w/c ratio is below 0.4, which corresponds to a mortar without capillary porosity [52]. On the other hand, with exception of ECM9, all the ECM mix designs with a w/c ratio exceeding 0.4 have an acceptable resistivity lower than 1000 Ω cm. The mix design ECM9 with a w/c ratio of 0.83, which has a resistivity of about 4000 Ω cm, showed a relatively weak compressive strength (9.8 MPa) with respect the other ECM, which indicates that possible microcrack may have occurred during temperature changes. Finally, as shown in Fig. 8c, for low resistivity range, no correlation is visible for both ECM and ECC. Yet, in the limited range of w/ c = 0.5–0.7, the resistivity of the ECC and ECM mix designs depends less on the w/c ratio, but more on the kinds of conductive inclusions.

The w/c ratio seems to have an effect on the ECM resistivity up to w/c of about 0.42. Below this value, the electrical conductivity does not seem to depend on the w/c ratio. The percolation of capillarity porosity allows the electrolytic ion conduction, which is one of the main mechanisms of electrical conduction of ECC.

4. Concluding remarks

This work aims at further developing ECC and ECM for heating system applications. Several ECC and an ECM mix designs have been investigated by combining copper powder, graphite powder, copper coated steel fibers, steel fibers, carbon fibers, graphene and conductive aggregates. Based on the present results, the following conclusions can be drawn:

(i) Several mix designs studied in this work showed an electrical resistivity (ρ_{TT}) after drying conditions which is suitable for de-icing applications threshold with satisfactory mechanical properties. In particular, ECC8 showed a satisfactory resistivity (215 Ω-cm) by combining 11%$_{vol}$ of GP and 1.4%$_{vol}$ of SF without the use of expensive CF. In comparison with previous ECC with same conductive inclusions [32], ECC8 employs much less volume content of SF, while guaranteeing similar resistivity. Moreover, ECC9 with a quaternary combination of conductive inclusions (18.2%$_{vol}$ CA, 10.8%$_{vol}$ GP, 1.36%$_{vol}$ SF and 0.1%$_{vol}$ graphene), showed a very low resistivity (i.e., 177 Ω cm) with a compressive strength of 24 MPa and a splitting tensile strength of 2.7 MPa. Finally, the mix design ECM4 (6.0%$_{vol}$ GP, 0.4%$_{vol}$ CF, 1.2%$_{vol}$ SF and 0.25%$_{vol}$ graphene) showed the best compromise between strength and electrical conductivity with a resistivity of 890 Ω cm and a compressive strength of 56.8 MPa. In general, graphite powder (GP) efficiently reduces electrical resistivity, but it reduces the compressive and splitting tensile strength due to the amount of absorbed water. When GP is employed, it is then important to optimize the water dosage to insure satisfying mechanical properties and to meet the de-icing resistivity threshold. The addition of steel fibers partially compensates such loss of mechanical strength;

(ii) The addition of a limited amount of graphene to ECC with other conductive inclusions was found to have a remarkable effect on the electrical conductivity, especially in dried condition. Synergistic effects between graphene and other conductive inclusions may be possible and should be further investigated;

(iii) Curing was found to have a important effect on the ECC conductivity which may explain the incongruency between laboratory and real field tests reported in previous works [11,16]. In general, drying increased the ECC resistivity, but this change is most reversible as shown by a further cure at high RH. The effect of RH and temperature on ECC electrical properties is then an important factor to take in account in real applications;

(iv) The w/c ratio plays a major role on the electrical conductivity of ECC and ECM. In general, for mix designs with w/c higher than 0.42, the water of capillary pore significantly contributes to the overall electrical conductivity. Moreover, by comparing results of ECM and ECC, it seems that the water porosity of the ITZ may play an important role on the overall electrically conductivity;

(v) A simplified model was able to predict the mean resistivity of ECC mix designs with satisfactory results.

Future research is needed to better understand the intrinsic resistivity of conductive materials and the contribution of the water porosity on the overall electrical conductivity of ECC. Moreover, a statistical study with a large number of samples is necessary to estimate the result dispersion and possible uncertainty

due to different casting methods. Finally, the durability of the developed ECC and ECM mix designs shall be verified.

Declaration of Competing Interest

The authors declare that they have no known competing financial interests or personal relationships that could have appeared to influence the work reported in this paper.

Acknowledgment

We would like to acknowledge the National Sciences and Engineering Research Council of Canada (NESRC) for the financial support through its EGP program (EGP 500750-16), Mitacs Accelerate program (internship No. 116843) and the Research Center on Concrete Infrastructures (CRIB). We would also like to acknowledge Ms. Sylvie Girard of Beton MultiSurfaces for the material donations and financial support to the project.

Annex A

Photos of the ECM sample sections.

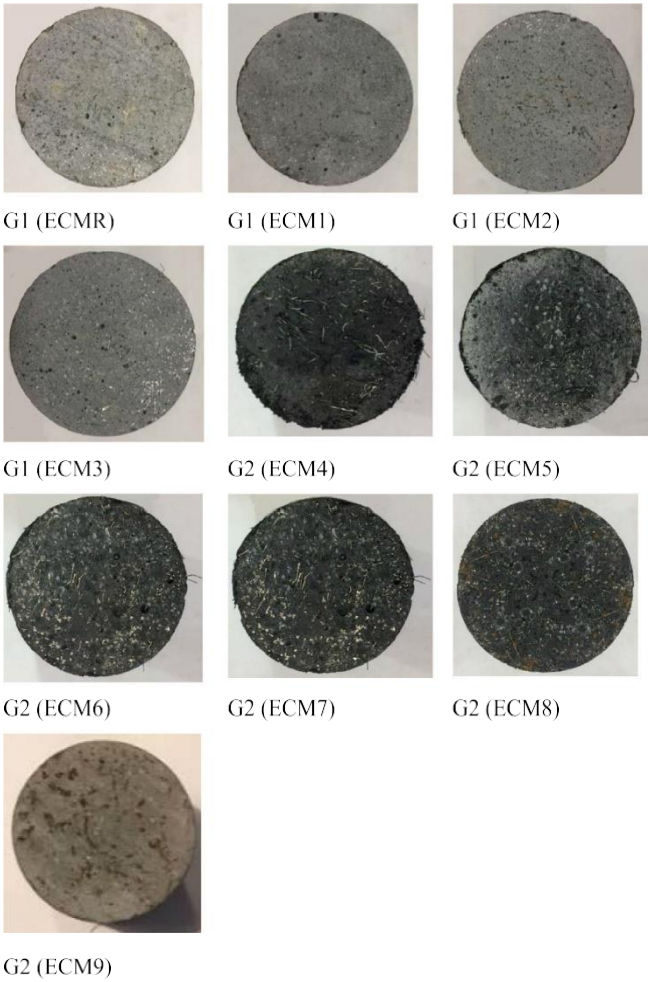

Photos of ECC sample sections

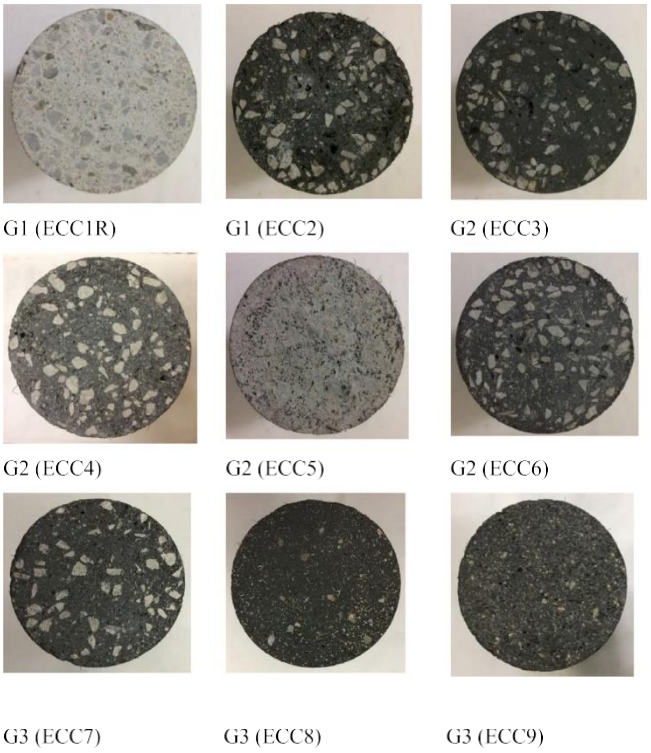

References

[1] Ouranos, Vers l'adaptation. Synthèse des connaissances sur les changements climatiques au Québec. Partie 1 : Évolution climatique au Québec. Édition 2015. Montréal, Québec : Ouranos, 2015 114p.
[2] K. Simonson, Percentage Change in Producer Price Indexes (PPIs) and Employment Cost Indexes (ECIs) for Construction, 2012–2017, Associated General Contractors of America, 2016.
[3] PhysOrg.com, Researchers develop solar-powered runway anti-icing system [Internet]. 2011 [cited 2017 Dec 7]. Available from: https://phys.org/news/2011-11-solar-powered-runway-anti-icing.html.
[4] R. Bruemmer, Montreal snow clearing: Better technology, more bike paths aim to blunt winter's sting, Montreal Gazette (2016).
[5] S. Yehia, C. Tuan, Thin conductive concrete overlay for bridge deck deicing and anti-icing, Transp. Res. Rec. J. Transp. Res. Board 1698 (2000) 45–53.
[6] Victoria R.K., Findlay S.E.G., Schlesinger W.H., Menking K., Chatrchyan A.M. Road salt moving toward the solution [Internet]. The Cary Institute of Ecosystem Studies; [cited 2018 Apr 3]. Available from: http://www.caryinstitute.org/sites/default/files/public/downloads/report_road_salt.pdf.
[7] A. Sassani, H. Ceylan, S. Kim, A. Arabzadeh, P.C. Taylor, K. Gopalakrishnan, Development of carbon fiber-modified electrically conductive concrete for implementation in Des Moines International Airport, Case Stud. Constr. Mater. 8 (2018) 277–291.
[8] S.A. Ketcham, E.J. Fleege, L.D. Minsk, R.R. Blackburn, Manual of Practice for an Effective Antiicing Program: A Guide for Highway Winter Maintenance Personnel. FHWA, Report No. FHWA-RD-9-202, 1996.
[9] H. Wang, L. Liu, Z. Chen, Experimental investigation of hydronic snow melting process on the inclined pavement, Cold Reg. Sci. Technol. 63 (1–2) (2010) 44–49.
[10] P. Pan, S. Wu, Y. Xiao, G. Liu, A review on hydronic asphalt pavement for energy harvesting and snow melting, Renew. Sustain. Energy Rev. 48 (2015) 624–634.
[11] H. Abdualla, H. Ceylan, S. Kim, K. Gopalakrishnan, P.C. Taylor, Y. Turkan, System requirements for electrically conductive concrete heated pavements, Transp. Res. Rec. J. Transp. Res. Board 2569 (2016) 70–79.
[12] Y. Lai, Y. Liu, D. Ma, Automatically melting snow on airport cement concrete pavement with carbon fiber grille, Cold Reg. Sci. Technol. 103 (2014) 57–62.

[13] S.A. Yehia, Airfield Pavement Deicing with Conductive Concrete Overlay, Env. Sci. (2002).
[14] P. Azarsa, R. Gupta, Electrical resistivity of concrete for durability evaluation: a review, Adv. Mater. Sci. Eng. (2017).
[15] I. Rhee, J.S. Lee, Y.A. Kim, J.H. Kim, J.H. Kim, Electrically conductive cement mortar: incorporating rice husk-derived high-surface-area graphene, Constr. Build. Mater. 125 (2016) 632–642.
[16] A. Sassani, H. Ceylan, S. Kim, K. Gopalakrishnan, A. Arabzadeh, P.C. Taylor, Influence of mix design variables on engineering properties of carbon fiber-modified electrically conductive concrete, Constr. Build. Mater. 152 (2017) 168–181.
[17] P. Xie, P. Gu, J.J. Beaudoin, Electrical percolation phenomena in cement composites containing conductive fibres, J. Mater. Sci. 31 (15) (1996) 4093–4097.
[18] P. Xie, J.J. Beaudoin, Electrically conductive concrete and its application in deicing, ACI Spec. Publ. 154 (1995). 399–399.
[19] H.W. Whittington, J. McCarter, The conduction of electricity through concrete, Mag. Concr. Res. 33 (114) (1981).
[20] N. Banthia, S. Djeridane, M. Pigeon, Electrical resistivity of carbon and steel micro-fiber reinforced cements, Cem. Concr. Res. 22 (5) (1992) 804–814.
[21] Z. Hou, Z. Li, J. Wang, Electrical conductivity of the carbon fiber conductive concrete, J. Wuhan Univ. Technol.-Mater. Sci. Ed. 22 (2) (2007) 346–349.
[22] C.Y. Tuan, Implementation of conductive concrete for deicing (Roca Bridge), Nebraska Department of Transportation Research, Report No 2008 (7-2008) 155p.
[23] J. Wu, J. Liu, F. Yang, Three-phase composite conductive concrete for pavement deicing, Constr. Build. Mater. 75 (2015) 129–135.
[24] B. Han, S. Ding, X. Yu, Intrinsic self-sensing concrete and structures: a review, Measurement 59 (2015) 110–128.
[25] F. Azhari, N. Banthia, Cement-based sensors with carbon fibers and carbon nanotubes for piezoresistive sensing, Cem. Concr. Compos. 34 (7) (2012) 866–873.
[26] B. Han, X. Yu, J. Ou, Self-Sensing Concrete in Smart Structures, Butterworth-Heinemann, 2014.
[27] B. Han, L. Zhang, J. Ou, Influence of water content on conductivity and piezoresistivity of cement-based material with both carbon fiber and carbon black, J. Wuhan Univ. Technol.-Mater. Sci. Ed. 25 (1) (2010) 147–151.
[28] B. Han, X. Yu, J. Ou, Effect of water content on the piezoresistivity of MWNT/cement composites, J. Mater. Sci. 45 (14) (2010) 3714–3719.
[29] F.J. Baeza, E. Zornoza, L.G. Andión, S. Ivorra, P. Garcés, Variables affecting strain sensing function in cementitious composites with carbon fibers, Comput. Concr. 8 (2) (2011) 229–241.
[30] J. Côté, J.-M. Konrad, A generalized thermal conductivity model for soils and construction materials, Can. Geotech. J. 42 (2) (2005 Apr) 443–458.
[31] P. Xie, P. Gu, Y. Fu, J.J. Beaudoin. Conductive cement-based compositions Google Patents, 1995.
[32] S. Yehia, C.Y. Tuan, D. Ferdon, B. Chen, Conductive concrete overlay for bridge deck deicing: mixture proportioning, optimization, and properties, ACI Mater. J. Apr (2000) 172–181.
[33] J. Rumble, Properties of Commercial Metals and Alloys, CRC Handbook of Chemistry and Physics, CRC Press/Taylor & Francis, Boca Raton FL, 2018.
[34] X. Liang, L. Ling, C. Lu, L. Liu, Resistivity of carbon fibers/ABS resin composites, Mater. Lett. 43 (3) (2000) 144–147.
[35] M.-S. Cao, X.-X. Wang, W.-Q. Cao, J. Yuan, Ultrathin graphene: electrical properties and highly efficient electromagnetic interference shielding, J. Mater. Chem. C 3 (26) (2015) 6589–6599.
[36] R.A. Matula, Electrical resistivity of copper, gold, palladium, and silver, J. Phys. Chem. Ref. Data 8 (4) (1979) 1147–1298.
[37] S. Türkel, V. Alabas. The effect of excessive steam curing on Portland composite.pdf [Internet]. Cement and Concrete Research 35 405-411; 2005. Available from: http://www.sciencedirect.com/science/article/pii/S0008884604003576?via%3Dihub.
[38] B. Graybeal, J. Hartamann, V. Perry, Ultra-high performance concrete for highway bridge, Symposium, FIB, Avignon, 2004.
[39] ASTM Standard C39/C39M-17b, Standard Test Method for Compressive Strength of Cylindrical Concrete Specimens, ASTM International West, Conshohocken PA, 2017.
[40] ASTM Standard C496/C496M-17, Standard Test Method for Splitting Tensile Strength of Cylindrical Concrete Specimens, ASTM International West Conshohocken PA 2017.
[41] M. Weber, M.R. Kamal, Estimation of the volume resistivity of electrically conductive composites, Polym. Compos. 18 (6) (1997) 711–725.
[42] L.E. Nielsen, The thermal and electrical conductivity of two-phase systems, Ind. Eng. Chem. Fundam. 13 (1) (1974) 17–20.
[43] P. Lura, O.M. Jensen, K. van Breugel, Autogenous shrinkage in high-performance cement paste: an evaluation of basic mechanisms, Cem. Concr. Res. 33 (2) (2003) 223–232.
[44] W. Wilson, V. Labattaglia, A. Tagnit-Hamou, L.S. Will, Blended-Cement Systems with Similar ASTM C1202 Chloride Penetration Potentials Resist Similarly to Corrosion?, Sixth International Conference on the Durability of Concrete Structures, Leeds, 2018.
[45] D. Dimov, I. Amit, O. Gorrie, M.D. Barnes, N.J. Townsend, A.I. Neves, et al., Ultrahigh performance nanoengineered graphene–concrete composites for multifunctional applications, Adv. Funct. Mater. 28 (23) (2018).
[46] S. Sun, B. Han, S. Jiang, X. Yu, Y. Wang, H. Li, et al., Nano graphite platelets-enabled piezoresistive cementitious composites for structural health monitoring, Constr. Build. Mater. 136 (2017) 314–328.
[47] Md. Safiuddin, M. Yakhlaf, K.A. Soudki, Key mechanical properties and microstructure of carbon fibre reinforced self-consolidating concrete, Constr. Build. Mater. 164 (2018) 477–488.
[48] B.A. Graybeal. Material Property Characterization of Ultra-High Performance Concrete, No. FHWA-HRT-06-103, 2006 186p. Available from: https://trid.trb.org/view.aspx?id=798080.
[49] W. Piasta, B. Zarzycki, The effect of cement paste volume and w/c ratio on shrinkage strain, water absorption and compressive strength of high performance concrete, Constr. Build. Mater. 140 (2017) 395–402.
[50] R. Kumar, B. Bhattacharjee, Porosity, pore size distribution and in situ strength of concrete, Cem. Concr. Res. 33 (1) (2003) 155–164.
[51] C. Lian, Y. Zhuge, S. Beecham, The relationship between porosity and strength for porous concrete, Constr. Build. Mater. 25 (11) (2011) 4294–4298.
[52] S. Mindess, J.F. Young, Concrete, Prentince-hall Inc., 1981.